Design, Fabrication and Testing a Semi-Automatic Sewing Device for Personalized Stent Graft Manufacturing

Yang Hu, Lin Zhang, Carlo A. Seneci, Wei Li, Mohamed E. M. K. Abdelaziz and Guang-Zhong Yang, *Fellow, IEEE*

***Abstract*—For the treatment of Abdominal Aortic Aneurysm (AAA), a personalised stent graft is used to ensure it fits tightly to the patients vessel geometry. A personalised stent graft is usually handmade which requires thousands of stitches and can take weeks or even months to complete. This delay may expose the patient to the risk of aneurysm rupture. This paper presents a robotic sewing device that can enhance the stent graft sewing speed by providing automated needle manipulation. It simplifies the sewing process and has the potential to achieve fully automated stent graft manufacturing via a vision-guided system. The device features a sewing probe that can switch a double pointed semi-circular needle between two movable jaws. This forgoes the need for manual needle handling including grasping, driving rotation, releasing and re-grasping, which requires a high level of manual dexterity and attention. This paper presents the design of the device, its mechanical synthesis and experimental validation. The focus of the paper is on the linkage parameter optimisation and needle locking mechanism design. The proposed device has been fabricated using 3D rapid prototyping techniques, and its performance has been compared with the conventional manual sewing method. The experimental results show that the device can achieve a 30% reduction of the completion time for a stitching task while achieving better consistency and quality of the stitches.**

Fig. 1. Sewing a Stent Graft with the Proposed Device

I. Introduction

VASCULAR disease is a major contributor to cardiovascular deaths in the Western world. Endovascular therapy has transformed the management of vascular disease, with clear advantages in terms of reduced morbidity and mortality, especially in patients unable to withstand traditional open surgery due to co-morbidities. For the treatment of AAA, personalised stent grafts are required to fit the exact geometry of the patient. For complex aneurysms, fenestrated and branched endo-grafts are further required to ensure continued perfusion of renal and visceral vessels. Manufacturing of these personalised stent grafts remains a lengthy, expensive process as they are still fabricated mostly by hand. Solutions have been proposed proposed to manufacture off-the-shelf standardised stent graft with automated processes [1]. However, the use of standard stent grafts may lead to an inadequate seal of the aneurysm sac. Stent migration may also happen in the long-term. To overcome this problem, personalised, custom-made stent grafts with an exact fit to a patient's anatomy are emerging as an appealing solution. These personalised stent grafts with complex shapes feature thousands of stitches; assuring the sewing quality can be extremely costly and time consuming with existing techniques. Currently, manufacturing one such stent graft can take up to 6-12 weeks. The long delay in stent graft manufacturing might expose the patient to the risk of aneurysm rupture. The development of an automated sewing technique for custom stents would improve the state of the art manufacturing and help the patients more effectively with ad-hoc solutions. Recently, innovation in 3D sewing is an important topic for industrial manufacturing. Extensive research has been carried out for developing single sided sewing heads that can work on 3D objects with closed surfaces. For example, a two-needle-head RS 530 [2] (KSL Keilmann, Lorsch, Germany) has been developed for sewing fabric-reinforced structures of aircraft parts. Automated sewing has also been widely researched in the textile industry. Most of the existing research has been focused on incorporating sensors and robots into conventional sewing machines to automate a few specific processes. Relevant topics include fabric tension control for robot-assisted fabric feeding [3], sewing seam tracking using an optical sensor [3] or using a camera system [4], and multi-arm robotic sewing [5].

All authors are with the Hamlyn Centre for Robotic Surgery, Imperial College London, UK, e-mail: y.hu12, lin.zhang, carlo.a.seneci, wei.li16, m.abdelaziz16, g.z.yang@imperial.ac.uk

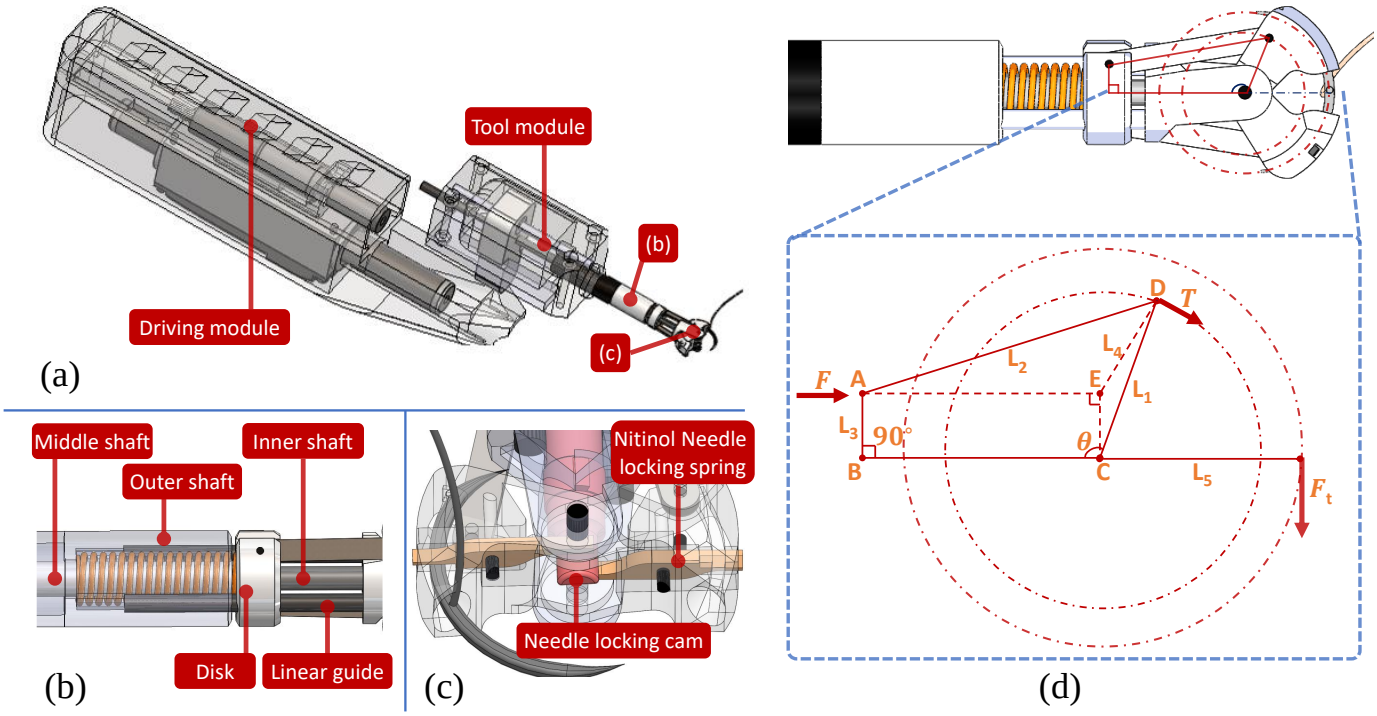

Fig. 2. (a) An overview of the sewing device. (b) The tool shaft. (c) The sewing probe. (d) An illustration of force transmission analysis for the slide-crank mechanism.

The use of threads to bind objects is not only employed in the field of textile industry. It has a wide range of applications in medicine. Due to the increased use of robotic-assisted systems in the field of minimally invasive surgery, various suturing devices that aim to automate the suturing procedure have been developed, including the Autosuture EndoStitch™ (Covidien, Dublin, Republic of Ireland) [6], the SILS™ Suturing Device (Covidien, Dublin, Republic of Ireland) [7], Endo360° Suturing Device, (EndoEvolution, Raynham, MA, US) [8], the PROXISURE™ Suturing Device (Ethicon, New Jersey, US) [9], the Switch® Suturing Device(Mellon Medical, Netherlands) [10] and the Eagle Claw endoscopic suturing device (Olympus Medical Systems Corp. Japan) [11]. According to the ways to operate the needle, these devices can be classified into two categories. For the first category, Switch®, EndoStitch™ and SILS™ systems switch a double pointed needle between two opposing jaws. A locking mechanism is built in each jaw to lock the needle. For the second category, devices such as Endo360° and PROXISURE™, work by continuously rotating a circular needle to perform stitching. Based on the aforementioned suturing devices, vision-guided robotic suturing systems, such as KidsArm Anastomosis Robot [12] and Smart Tissue Autonomous Robot (STAR) [13], [14], have demonstrated that it is feasible for a robot to perform anastomosis autonomously.

When comparing the aforementioned industrial sewing methods with surgical suturing, the industrial one usually relies on using a fixed sewing machine that rapidly produces only one specific type of stitch, while the surgical suturing is more versatile, which can perform various types of stitches as well as knot tying, albeit with slower speed. Furthermore, industrial sewing machines can be quite large and complex. They require synchronisation of the needle and bobbin in a sophisticated, perfectly matched timing sequence. Traditional sewing machines work only for flat sewing objects. The single-sided sewing head can perform sewing on the outer surface of generic 3D objects; however, these objects are relatively big and heavy. The surgical suturing devices have an advantage that they are relatively simple and compact, suitable for working in a confined space, such as a corner or a tight lumen. Finally, the stitch pattern of the industrial sewing machines is quite thick because two threads are usually interwoven to perform continuous sewing, while the surgical suturing only uses a single thread. For stent graft manufacturing, multiple stitch types are required which include running stitches along the stent and tying knots to fix the apexes of the sinusoidal-shaped stent. To access corners between the branches, the sewing device needs to have a small and compact footprint.

Based on the above considerations, the idea for developing the new sewing device for sewing stent graft was inspired mostly by the surgical suturing devices. In previous work [15], [16], [17], a vision-guided multi-robot manufacturing system for the flexible production of personalised medical stent grafts was proposed. It features two robotic arms each holding a surgical needle driver to perform the task. One drawback of this system is that it requires a frequent releasing and re-grasping of the suturing needle, which introduces a significant challenge for automating the task. In this paper, a patented sewing device (Fig. 1) developed by the authors is used for sewing personalised stent grafts.

The proposed device can not only be used as a hand-held device to increase manual stent graft sewing speed,

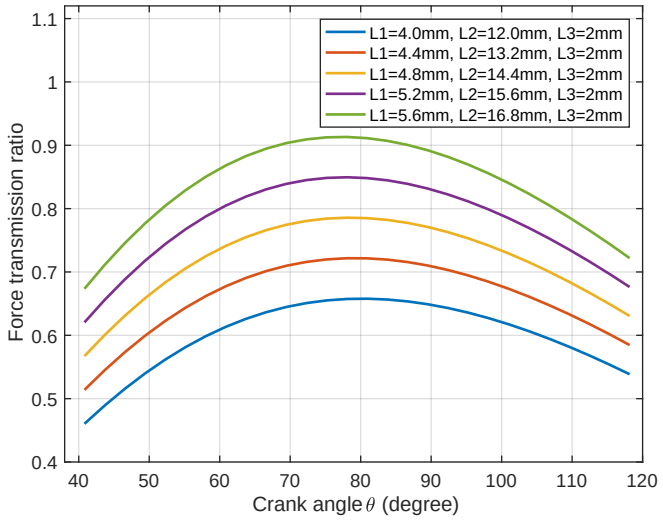

Fig. 3. Force transmission with changing of the crank angle in different L_1, L_2.

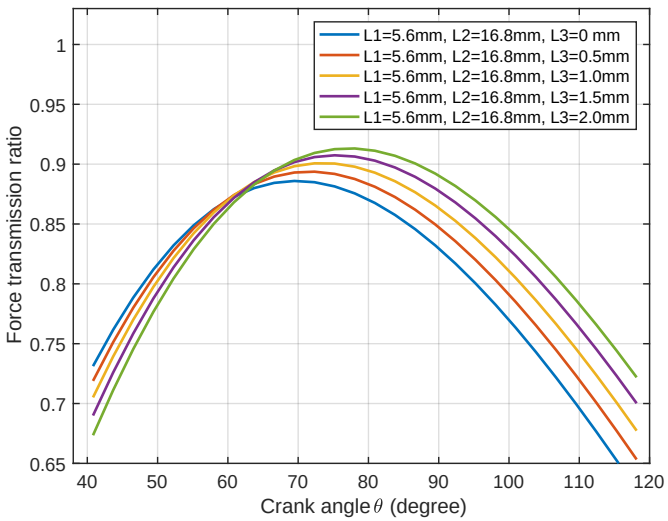

Fig. 4. Force transmission with changing of the crank angle in different L_3.

but also be integrated into a vision-guided robotic sewing system to achieve fully automated stent graft manufacturing [18]. Compared with the existing sewing/suturing systems, the proposed device has three distinctive features: Firstly, it is the first device which can switch a double pointed semi-circular needle to perform stitching. The needle moves by following its tangential direction, which is vital to guarantee a minimal tearing force applied to the object being sewed. Compared with the device using a straight needle, the proposed device is more suitable for sewing stent grafts because a curved needle can easily move around the stent without deforming the stent. Secondly, the needle has a large exposure area out of the device. Compared with the suturing devices whose needle is hiding inside the circular housing, the operator of the proposed device can use the needle tip as a reference for targeting a stitching point. Furthermore, the exposed needle tip can also be used to interact with the thread to perform knot tying. Thirdly, the needle is locked by only with friction such that no notches are required on the needle body, making the needle pierce through the object more smoothly.

The main contributions of this work are:

1) The proposition of a novel sewing device that is multi-functional, being possible to implement it in the textile and surgical industries. The device is versatile and can be used either for faster manual sewing or automated robotic sewing.
2) The mechanical synthesis and experimental validation of the device, ranging from the investigation of different link parameters for improving the performance of the needle driving mechanism to utilisation of FEA to assist the design of the NiTi needle locking mechanism.
3) The manufacturing of the proposed concept with various rapid-prototyping techniques, such as selective laser melting, laser cutting and electrical discharge machining.
4) Experimental validation with a detailed user study to verify usefulness of the proposed device.

II. Mechanical Design of the Sewing Device

A. Design Overview

An overview of the sewing device is shown in Fig. 2. The device consists of a tool module and a driving module. The tool module has an elongated body with the sewing probe at its distal end as shown in Fig. 2(c). The driving module consists of two motors and a mechanical interface for docking the tool module. The sewing probe can switch a double pointed semi-circular needle between two movable jaws. A thread is affixed to the middle of the needle. To switch the needle between the two jaws, the sewing probe has two DoFs: one for driving the jaws and passing the needle between the jaws; one for alternately locking the needle in each jaw. The two jaws are movable between an open position and a closed position. Each jaw contains a needle locking mechanism to hold the needle. When the first jaw holding the needle moves towards the closed position, the needle also moves and penetrates the object being sewed between the two jaws. After the needle pierced through the fabric layer, its tip begins to enter the second jaw until the jaws are fully closed. At this stage, the locking mechanism in the first jaw is released and its counterpart, in the second jaw, is engaged. The needle is then retrieved by the second jaw when the jaws move towards the open position. Since the semi-circular needle is fixed coaxially with the pivot of the jaws, the needle is rotated around its geometrical centre during the piercing process. This feature guarantees a minimal tearing force applied to the object being sewed. In order to make the design compact, a rigid slider-crank mechanism is utilised to drive the two jaws. The mechanism converts a reciprocating, linear sliding motion at the tool's proximal end to a rotational movement at the tool's distal end. As shown in Fig. 2(b), the tool's shaft consists of three layers:

1) The inner shaft is a rod with a semicircular cam at the distal end for locking the needle;
2) The middle shaft is a tube connected to a disk for driving the slider-crank mechanism;

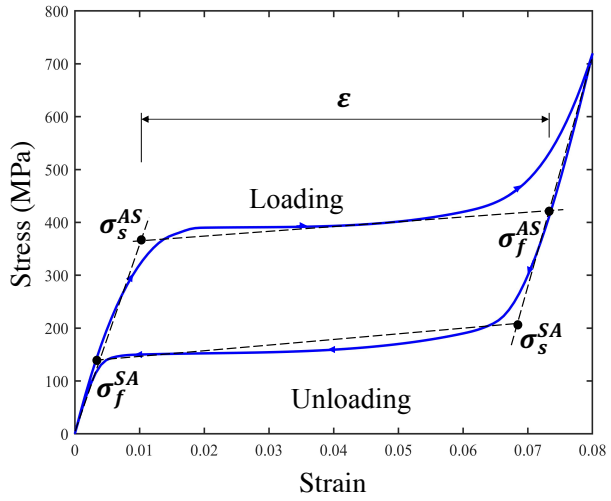

Fig. 5. The strain-stress relation of the NiTi alloy.

3) The outer shaft is a tube for supporting the whole structure.

B. Needle Driving Mechanism Design

In order to overcome the friction required for the needle to penetrate the object being sewed and enter in the needle channel, the needle driving mechanism requires a high force transmission ratio from the motor to the needle, as shown in Fig. 2(d). For optimising the force transmission ratio of the slider-crank mechanism, there are three parameters to tune: the crank length L_1, the coupler length L_2, and the offset length L_3. In order to achieve a low fluctuation in velocity, L_2 should be at least three times greater than L_1 [19]. On the other hand, L_1 and L_2 should not be excessively long to achieve a compact design. Therefore, L_2 is set as three times of L_1.

A force transmission analysis is carried out with the two independent parameters: the crank length L_1 and the offset length L_3, as depicted in Fig. 2(d). In Fig. 2(d), θ is the angle between the crank link and the central axis of the tool shaft, L_5 is the radius of the needle, F is the input force from the motor. T is the torque applied to the crank by the coupler, which drives the jaws and F_t is the tangential force of the needle tip. R is The force transmission ratio R can be calculated via triangle geometry. For detailed derivation of R please refer to Appendix.

Fig. 3 illustrates the effect of varying the crank length L_1 ($L_2 = 3L_1$) on the force transmission ratio R. Fig. 4 illustrates the effect of the offset length on R. These graphs show that a longer L_1 will result in a larger R. As illustrated in Fig. 3, at $\theta = 80°$, R is increased by approximately 40% as L_1 is increased from 4 mm to 5.6 mm. As shown in Fig. 4, the maximal R can be achieved when L_3 is 2 mm and $\theta = 75°$. In order to overcome the friction to enter the opposite jaw, the needle locking mechanism is required to have a large force transmission ratio R when the jaws are near the closed position. Therefore L_1 and L_3 are selected both as their maximal values, 5.6 mm and 2 mm respectively. The allowable ranges for L_1 and $L3$, which will be experimentally validated in Section III, are 4-5.6 mm and 0-2 mm respectively.

TABLE I
KEY FEA STATISTICS FOR EACH DESIGN.

	Max Strain	Force on the needle(N)	Force to strain ratio
Design 1	1.6%	11.7	731.2
Design 2	2.6%	39.7	**1526.9**
Design 3	3.6%	48.8	1355.5
Design 4	4.2%	52.0	1238.0

C. Needle Locking Mechanism Design

Most of the existing sewing devices use customised needles that feature notches, either for locking the needle in position or driving the needle. Creating notches on the needle surface weakens itself, and also reduces the needle's smoothness, as well as increases manufacturing complexity. In our design, the needle is locked in position by using only friction. The locking mechanism is shown as Fig. 2(c). It comprises a rotational cam and two flat springs (one in each jaw). The flat spring works like a lever with the pivot located at its centre. The rotational cam has a semi-circular profile. When it engages with one end of the flat spring, the other end of the spring is pressed onto the needle to keep the needle in position. With a $180°$ rotation of the cam, the needle can be locked at the other jaw. When the needle is in the locked status, the flat spring is deformed by the physical constraints of the cam and the needle, so a large force can be applied on the needle.

The flat spring used is made from a super-elastic NiTi alloy, which can recover to its original shape after a substantial bending. According to literature [20], the NiTi alloy usually has a maximal strain of around 6% which is much larger than other metals, such as steel (maximum strain around 0.5%). The strain-stress curve of the NiTi alloy, illustrated in Fig. 5, shows the hysteresis effect of the NiTi alloy. When stress is applied to the NiTi alloy, it transforms from the austenite phase to the martensite phase. Once the stress is removed, it returns to the austenite phase. The austenite-to-martensite transformation can also happen during dramatic temperature changes. In the proposed design, we only use its super-elastic property rather than its thermal-mechanical property, so the super-elastic NiTi alloy with transformation temperature significantly lower than a typical medical application is chosen.

The main design principle for the shape of the flat spring is to reduce its maximum strain during the operation (requiring a thinner spring) and at the same time to generate larger force applied on the needle (requiring a thicker spring). The flat spring should have a uniform and smooth body shape to prevent stress concentration. Fig. 6 shows the FEA results created by the ANSYS® software (version 18.2) for four spring designs with the strain stress parameters are shown in Fig. 5. The first one is a basic design with a constant radius fillet in the corner. The strain mainly concentrates on the transition area of this design. For design 2, 3 and 4, in order to distribute the strain more evenly, the areas with the minimal strain (the blue area in design 1) are removed, including the left-up corner and the inner cut area. The shape

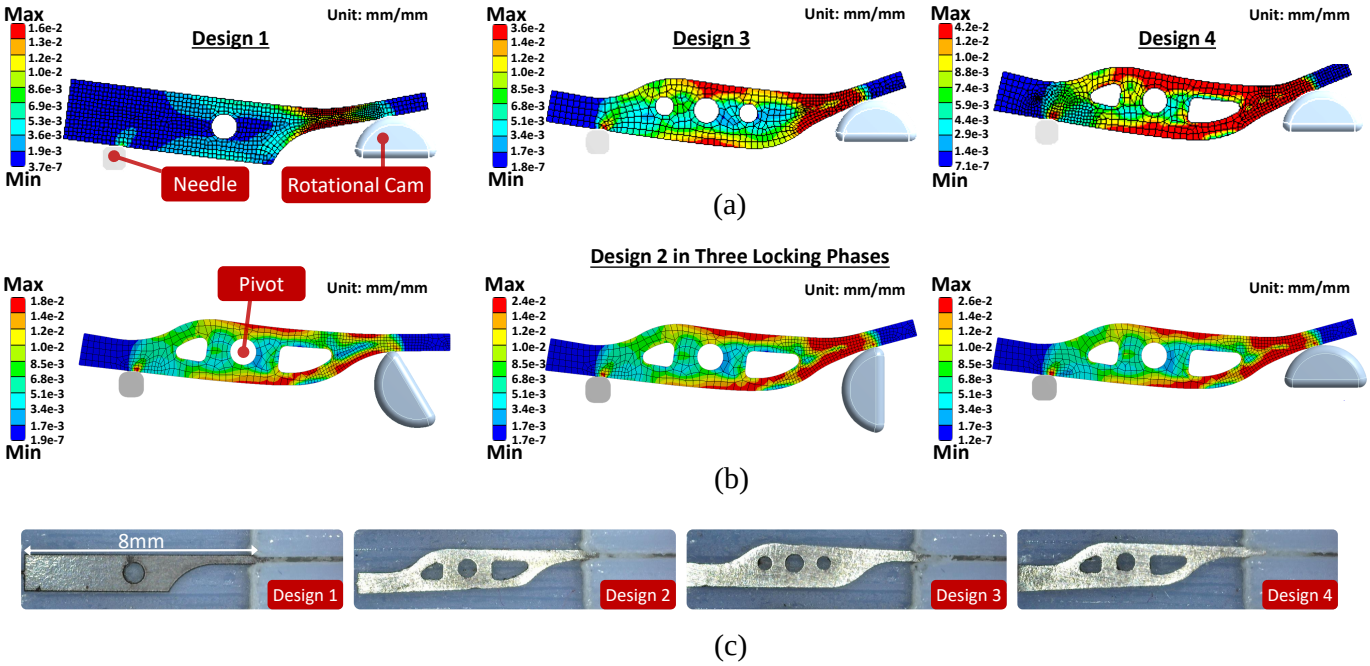

Fig. 6. FEA results of the strain distribution in four different flat spring designs. The flat spring rotates around the pivot (the circle in the centre of the spring), and it is deformed by the needle and the semi-circular rotational cam. (a) The stain distribution for Design 1,2 and 3 when the needle is in locking status. (b) The strain distribution for Design 2 in three locking phases. (c) The four NiTi flat spring samples made by laser cutting.

of the transition area is also redesigned using the method of tensile triangles [21], which mimics the shape of the tree buttress to reduce stress concentration. Design 2 and design 3 have the same outlines, but their inner cuts are different. The design 4 is same with design 2 except that it is thicker. The analysis results in Table. I show the maximal strain for each design. The force applied on the needle is also reported in our simulation. As the strain increases, the force applied on the needle also increases. The force to strain ratio is also shown in Table. I. Design 2 has the largest force to strain ratio among the four designs, so it might be a good option, which will be evaluated in the experiment. Fig. 6(b) shows three locking phases for design 2. The maximal strain is experienced when the circumference of the rotating cam contacts with the flat spring. The FEA results show that when the shape of flat spring becomes more uniform (compared Design 2, 3, 4 with 1), the strain and stress distribute more evenly. As the spring becomes thicker, the force applied on the needle as well its maximal strain are also increased.

D. Driving Module and Control

The driving module consists of two motors: a linear DC servomotor (LM 2070, Quickshaft, FAULHABER GmbH & Co. KG) and a brushless DC servomotor (1226, gearbox ratio 16:1, FAULHABER, GmbH & Co. KG). The linear servomotor is used for controlling the needle driving mechanism, and the brushless DC servomotor is used for controlling the needle locking mechanism. The control system consists of two FAULHABER motion controllers (MCLM 3006 linear motor controller and MCBL 3006 brushless motor controller) connected to a host computer via a RS-232 interface.

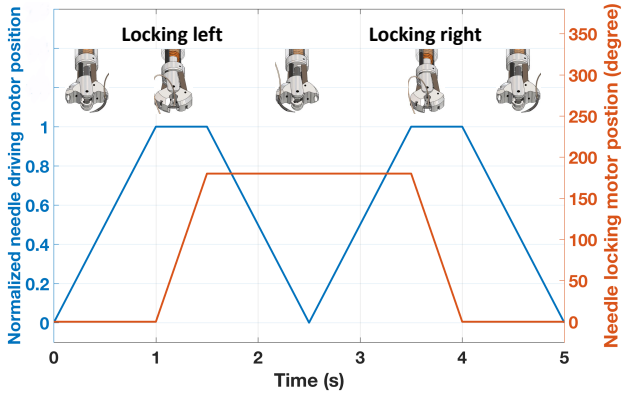

Fig. 7. One complete working sequence of the sewing device.

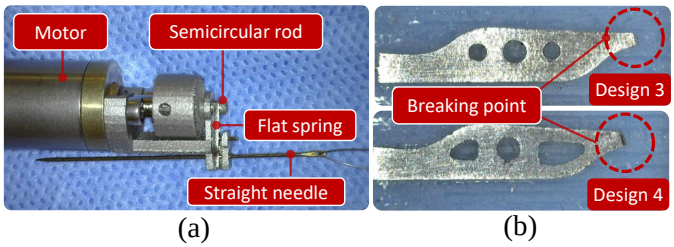

Fig. 8. (a) The test rig which uses the same flat spring as the suturing device. (b) Design 1 and Design 2 survived after the 1000 cycles test while Design 3 and Design 4 broke during the test. The broken parts of Design 3 and Design 4 are highlighted.

The motion controllers are responsible for the low-level PID control while the software running in the host computer provides supervisory commands, such as moving forward or stop. The current consumption of the motor is monitored at 80 Hz. This information can be used to detect whether the motor has reached a hard stop. More specifically, the motor consumes more current when a larger payload is applied. In the calibration procedure, current sensing is used to find the physical constraints of the range of motion of the actuators. During the sewing process, the current sensing is also used to monitor the situation when the needle is inadvertently bent. Friction would increase excessively, triggering a failure signal. When the device is used in a hand-held configuration, it is controlled with a foot pedal. By pressing the foot pedal, the device switches the needle between the two jaws. The locking of the needle is controlled automatically according to the position of the needle, without requiring additional user inputs. A complete working sequence of sewing device can be illustrated in Fig. 7.

E. Manufacturing

3D rapid prototyping techniques are used to manufacture the proposed sewing device. The semi-circular needle is with 6.0 mm radius and 0.55 mm thickness. Instead of having only one sharp tip and the thread is attached to the other end, the proposed needle features double sharp tips and the thread is clamped in the middle of the needle. Electrical Discharge Machining (EDM) technique (Sarix 3D EDM Milling Machine, Sarix SA, Switzerland) is used to produce the proposed double-pointed semi-circular needle and create a 0.25mm thread eyelet in the middle of the needle body to pass and secure a nylon thread. The stainless-steel components of the sewing device are manufactured by Selective Laser Melting (SLM) (Mlab cusing R, Concept Laser GmbH, Germany). The flat spring used for locking the needle is laser cut (MPS 3D-Modular Processing System, ROFIN-BAASEL Lasertech GmbH, Germany) from a NiTi sheet (Memry Corporation, US). The NiTi sheet is 0.5mm thick with the superelastic property, and it has a transition temperature around $-15°$, which is below the required application temperature of this device. The major cost of the sewing device is the motors and the corresponding controllers, which is approximately 3000 dollars in total. The cost of the material used for producing the components is low (less than 10 dollars).

III. Experiments and Results

A. Force Transmission Experiment

According to the force transmission analysis in Section II B, we found that increased L_1 and L_3 can result in an increased force transmission ratio R; however, this also makes the design less compact. This experiment was designed to test the necessity of increasing L_1, L_2 and L_3. In the experiments, we used a force gauge to push the slider (the disk) of the slider-crank mechanism to close the jaws. A torsional spring was put between the two jaws. The force (F_t) required to compress the torsional spring is 5.0N. The maximum pushing force for each set of parameters was recorded during the process. In the experiment, five sets of link lengths were tested. The link length parameters and the recorded force are shown in Table II. The maximal measured force transmission ratio and the maximum predicted force transmission ratio (obtained from the analysis in Section II-B) are also listed. When the link length of L_1 increased by 20.0% and by 40.0% in the case 2 and 3 compared with the case 1, the maximal measured force transmission ratio is increased by 18.6% and by 35.6% respectively. Varying the length of L_3 also slightly increases the force transmission ratios. Also, due to the influence of friction, the maximal measured force transmission ratio is 0.07-0.12, which is lower than the predicted one. According to the study, the longer the links length L_1,L_2 and L_3, the less force is required to close the jaws. Friction influences the force transmission, but the link parameters are still the major decisive factor. So, L_1, L_2 and L_3 has been designed as 5.6mm, 16.8mm and 2mm, respectively. These are the maximal values within each allowable range.

TABLE II
Test the force transmission in different link lengths.

	L_1	L_2	L_3	F	F_t	Max Mea.R	Max Pre.R
Case 1	4.0	12.0	2.0	8.4	5.0	0.59	0.66
Case 2	4.8	14.4	2.0	7.1	5.0	0.70	0.78
Case 3	5.6	16.8	2.0	6.2	5.0	0.80	0.92
Case 4	5.6	16.8	1.0	6.5	5.0	0.78	0.90
Case 5	5.6	16.8	0.0	6.7	5.0	0.75	0.86

*The unit for L_1, L_2 and L_3 is millimetre. The unit for F and F_t is Newton.

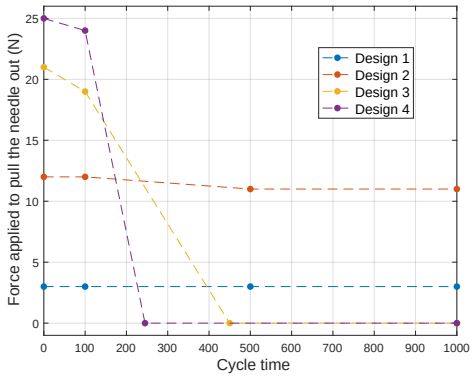

Fig. 9. This plot shows the result of 1000 locking/unlocking cycles test for the flat springs. In the locking status, the force required to pulling the needle out was measured at 0, 100, 500 and 1000 cycles. The Design 3 broke after 450 cycles and Design 4 broke after 245 cycles, so their corresponding pulling forces were set as 0 after the failure

B. Flat Spring Experiment

The samples for the four designs analysed in Section II-C. are shown in Fig. 6(c). A needle locking test rig, as shown in Fig. 8 with the same geometry as the sewing device was used to test these springs. The semi-circular cam used for locking the needle was connected to the motor shaft directly. The circular needle was replaced with a straight needle for easily measuring the force used for pulling the needle out. Fig. 9 shows the result after 1000 locking/unlocking cycles for the four designs. For Design 1 and Design 2, the force was constant throughout the test: 3N for Design 1 and 12N

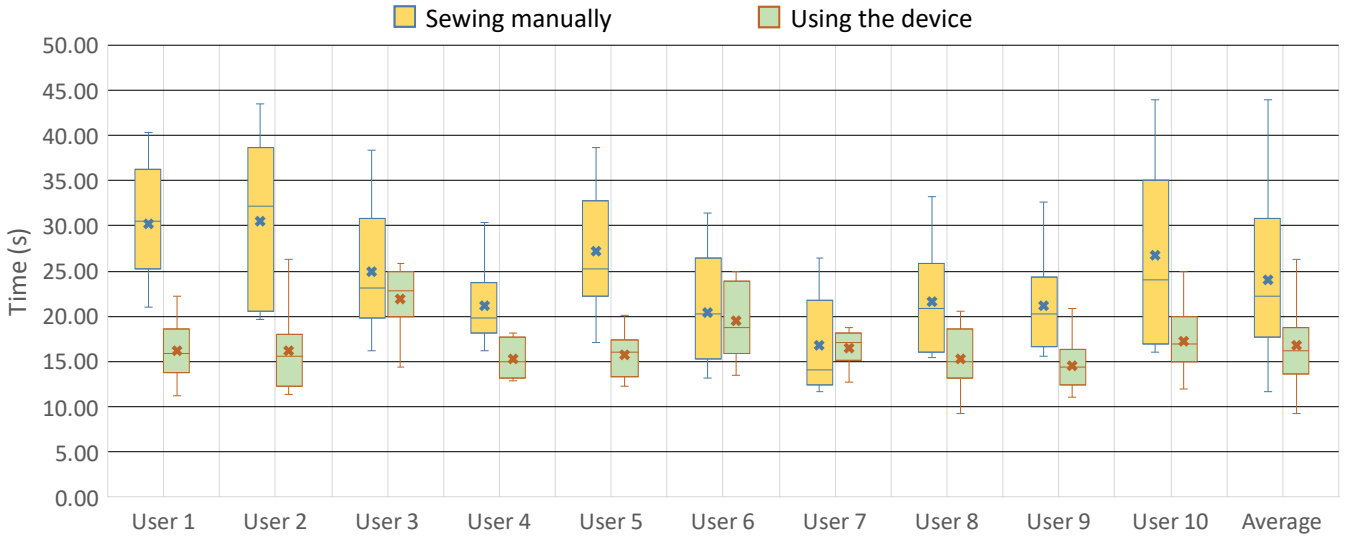

Fig. 10. Box plot of the experiment results. The first 10 pairs of box plots illustrate the time distribution of performing one stitch in both manual and semi-automatic task for each user. The last pair of plots illustrate the combined results for all the users.

for Design 2. For Designs 3 and 4, they demonstrated a larger force for locking the needle at the beginning of the test. However, both failed the test as shown in Fig. 8(b). The breaking point is located at the place of stress concentration which is visible from the FEA results in Fig. 6. The presence of stress concentration caused by cyclical loading is the main reason which causes fatigue of the NiTi alloy. Another reason is the use of laser cutting technique which may deteriorate the super-elastic properties of NiTi due to the heat generated in the alloy [22]. From the literature, the NiTi alloy may lose up-to 50% of original recovery strength after 10% of its cycle life; therefore, it is important to identify the optimal design trade-off that does not hinder the performance over time. Design 2 has been finally selected to be used in the sewing device, which has 3 times larger needle locking force than Design 1 and performs consistently over time. The selected spring design could further be improved and tested for longer life-cycles. Current design requires a 12 N force to pull the needle out even after 1000 cyclic loading, which already meets the requirement of our application.

C. Stent Graft Sewing Experiment and Results

To verify if the sewing performance can be improved by using the semi-automatic method (with the device) over using the manual method (with a needle holder), ten users (five males, five females) were asked to sew a stent (a sinusoidal metal ring) to a graft (a fabric tube) with both the manual method and semi-automatic method. Eight participants (user 1-5, 8-10) were novices without experience in suturing/sewing with a curved needle. User 6 is familiar with both the manual and semi-automatic method, while user 7 is only familiar with manually sewing stent grafts. Fig. 12(a) illustrates a stent, a graft and a 3D printed mandrel used in this study. The mandrel was used for holding the graft and the stent in place during the sewing experiment. The graft was warped onto the cylindrical surface of the mandrel which has a soft surface for providing appropriate tension on the fabric being sewed. The NiTi stent was placed outside the fabric tube.

In the manual sewing task, a microsurgical needle holder was used to operate a semi-circular needle. The sewing task was conducted in a bimanual fashion, where the user used one hand to hold the mandrel and the other hand to hold the needle driver. To perform one stitch, a user needs to release and re-grasp the needle twice. The first needle re-grasping operation happens when the user performs stitching and pulls out the needle, and the second operation occurs when the user adjusts the grasping position from the needle tip to the needle thread end to initiate next stitch. In the semi-automatic sewing task, the needle driver was replaced with the proposed sewing device. The same needle was automatically driven and switched between the jaws of the device, which was controlled by pressing a foot pedal. In both tasks, the users were asked to evenly apply blanket stitches along the sinusoidal shape of the stent. The blanket stitch can be simply made by passing the needle through the loop of the previous stitch.

Each user was given a short introduction and sewing demonstration (around five minutes) and they could practice fifteen stitches before performing the experiment. To remove the learning effect, five participants performed the manual sewing first, and the other five participants performed the semi-automatic sewing first. In the experiment, each user was asked to perform 20 stitches, the time for finishing each stitch was recorded. Fig. 10 utilises a box plot to show the experiment results. Firstly, it shows that for every user the average stitch completion time (cross symbol in the plot) with the semi-automatic method is shorter than the manual method. The decrease of the completion time ranges from 14.2s (user 2) to 0.3s (user 7). Although user 7 is familiar with manually sewing the stent graft and new to use the device, the subject still performed slightly faster when using the device.

During the experiment, the hand movement when using the sewing device and the needle driver were recorded by using a NDI Aurora tracking system with a 6-DoF sensor (accuracy

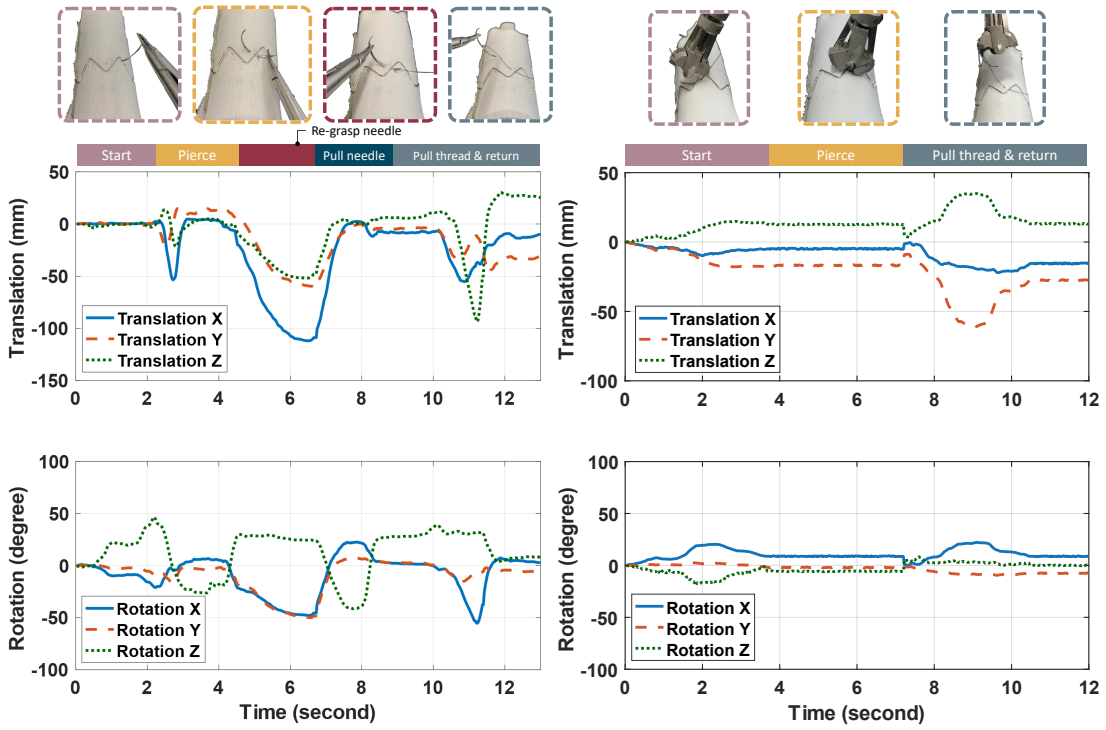

Fig. 11. This figure shows the trajectories of the sewing device and the needle holder recorded with NDI motion sensor. Position and orientation are displayed separately in the plots. (a) Manual trajectory. (b) Device trajectory.

around 1.8mm). The sensor was mounted closed to the holding position of both devices. Fig. 11 shows the hand trajectories of user 7 in both manual and semi-automatic tasks. By comparing the bottom two plots (rotation) in Fig. 11, we found that the manual sewing has two phases with significant orientation changing: one for pushing the needle in and the other for pulling the needle out. When using the device, the user's wrist movement could be avoided, resulting in no significant orientation change. Furthermore, the semi-automatic method requires less translational movement, because in manual sewing task, to initiate a new stitch, the user needs to put the needle in a convenient place to swap the holding position, while the semi-automatic sewing avoids this procedure. Looking at the average result for all users, the average completion time is 24.1 seconds (manual method) versus 16.8 seconds (semi-automatic method), which means using the device could increase around 30% of the sewing speed. In addition, for all the users, sewing with the device has a lower standard deviation than manual sewing. The main reason behind this is that the needle sometimes slipped or dropped during the manual task, introducing a 2s to 10s delay. For example, for user 2 and user 10, they found that it was difficult to use the needle holder to push the needle through the fabric. They tended to apply large force on the needle holder, making the needle slip out from the jaws. Another factor delaying manual sewing is that users had to adjust the needles orientation before insertion. The proposed device is not affected by these problems, the needle is held tightly by the device, and it takes consistently 1.6 seconds to finish one needle passing. Using the device, not only is the sewing speed faster, but also the performance variance across users is lower. Therefore, the manual method has a steeper learning curve, while the semi-automatic method is easier to master. Fig. 12(b) shows the sample sewed by user 7. The stitches on the upper stent were accomplished by using a manual method and the lower ones are the results of using the device. From the zoomed view, it is visible that the stitch quality regarding stitch size, tightness and consistency are similar between the manual and semi-automatic methods.

Although the sewing device has a promising performance, there are also some aspects that could be improved. Some users felt the device is heavy and may cause tiredness if used for a prolonged time. Also, user 10 did not hold the device steadily when the needle was passing through the fabric. The needle was therefore bent and failed to enter the opposing channel. The situation was detected by current monitoring routine in the software, the device was stopped, and the damaged needle was manually changed with a new one.

The Fig. 12(c) shows a commercial personalized stent graft. Blanket stitch is applied to finish the edge of fenestrations and scallops. Successive knot tying is used to secure the stent on the fabric. The commercial stent graft has more dense and consistent stitch patterns for securing the edge. There are several reasons. Firstly, the needle used for sewing the commercial stent graft is a surgical suture with the thread attached to one end of the needle. Compared with the proposed sewing device with thread attached to the middle of the needle, it causes less biting damage to the fabric, because the thread could follow the needle smoothly. Secondly, to achieve such high sewing quality, it requires a thinner needle and months of sewing training. Even though the performance of using the proposed device is not yet comparable with

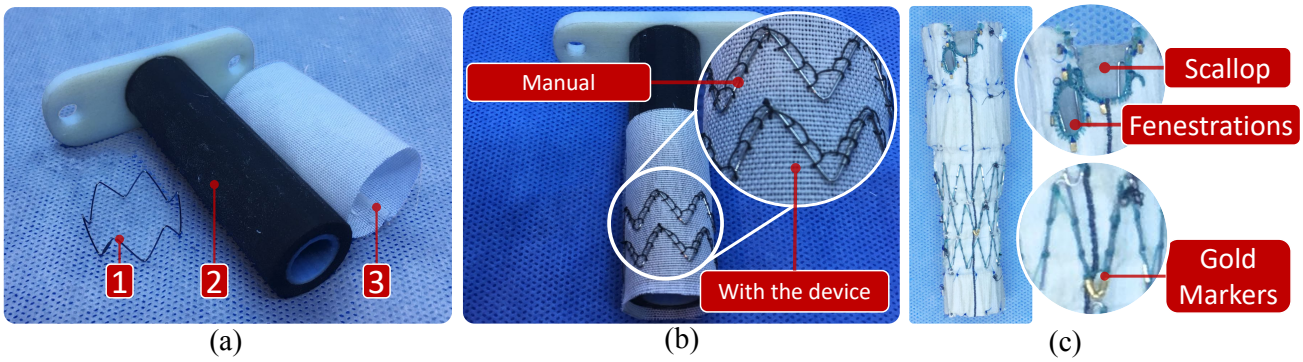

Fig. 12. (a) The material used in the sewing experiment: (1) A NiTi stent; (2) A 3D printed mandrel for holding the stent graft to be sewed; (3) A fabric tube. The frame of the mandrel is printed with a hard material (the white portion), and its cylindrical outer surface is printed with a soft material (the black portion). (b) One sample produced in the experiment. The stitches on the upper stent were applied using traditional technique and the lower one with the proposed device. (c) A commercial stent graft.

the commercial results, it shows a promising solution for automating the sewing procedure. As demonstrated in [18], this sewing device is integrated into a robotic sewing system to perform automated stent graft sewing. With closed-loop visual serving, novel thread manipulation method plus thread tension sensing, an automated knot tying procedure is also proposed and demonstrated.

IV. Conclusion

This paper demonstrates a novel sewing device that can automatically drive and lock a double-pointed semi-circular needle to perform sewing. The device ensures the needle can be grasped and locked in the same position. A slider-crank mechanism has been designed to achieve a compact footprint while providing sufficient force on the needle tip. A set of optimal link parameters has been selected to achieve lower velocity fluctuation on the actuation mechanism and higher force transmission ratio. Furthermore, a needle locking mechanism made by superelastic NiTi alloy has been designed which was tested with FEA to ensure the optimal trade-off between needle holding force and fatigue resistance. The experimental results verify that the semi-automatic sewing method using the proposed device has several advantages over the manual method in terms of completion time and consistent performance. Moreover, the proposed device can also facilitate fully automated sewing by mounting the device on a robotic arm, which can potentially reduce the cost of a personalised stent graft. Beyond the application used in this paper, the sewing device can also be used in surgery when it is designed as a laparoscopic or endoscopic tool.

Appendix
Derivation of the Force Transmission Ratio

From Fig.2(d), it can be derived that,

$$\angle ECD = |\theta - 90^\circ| \tag{1}$$

$$L_4 = \sqrt{{L_1}^2 + {L_3}^2 - 2L_1L_3\cos(\angle ECD)} \tag{2}$$

$$\angle CED = \pi - \arcsin(\frac{L_1\sin(\angle ECD)}{L_4}) \tag{3}$$

$$\angle AED = \begin{cases} \frac{3}{2}\pi - \angle CED, & \text{for } \theta \geq \frac{\pi}{2} \\ \angle CED - \frac{\pi}{2}, & \text{for } \theta < \frac{\pi}{2} \end{cases} \tag{4}$$

$$\angle EAD = \arcsin(\frac{L_4\sin(\angle AED)}{L_2}) \tag{5}$$

$$\angle ADC = 180^\circ - \angle EAD - \theta \tag{6}$$

$$F\cos(\angle EAD)L_1\sin(\angle ADC) = T = F_tL_5 \tag{7}$$

therefore, the force transmission ratio R can be expressed as:

$$R = \frac{F_t}{F} = \frac{L_1\sin(\angle ADC)\cos(\angle EAD)}{L_5} \tag{8}$$

Acknowledgment

This research was supported by the UK Engineering and Physical Sciences Research Council (EPSRC) with grant reference EP/L020688/1 and EP/P012779/1. We would like to thank Dr. Benny Lo, Dr. Su-lin Lee, Dr. Bidan Huang for their advice during this research. We thank Dr. Jindong Liu, Dr. Jianzhong Shang for their experience and insight in advising the mechanical design. We would like to thank David Williams and Pierre Berthet-Rayne for their help on operating the machines used in this research.

References

[1] P. Phillips, A. M. Woodward, A. R. B. Halket, G. Beaton, C. J. Perks, C. G. Angel, and T. F. Frost, "Method for manufacturing stent-grafts," Jul. 11 2006, uS Patent 7,073,456.

[2] "KSL Two needle head RS 530," http://www.ksl-lorsch.de/en/products/aerospace/aviation/two-needle-head-rs-530/, [Online; accessed 25-January-2018].

[3] J. Schrimpf, M. Bjerkeng, and G. Mathisen, "Velocity coordination and corner matching in a multi-robot sewing cell," in *Intelligent Robots and Systems (IROS 2014), 2014 IEEE/RSJ International Conference on*. IEEE, 2014, pp. 4476–4481.

[4] M. Kudo, Y. Nasu, K. Mitobe, and B. Borovac, "Multi-arm robot control system for manipulation of flexible materials in sewing operation," *Mechatronics*, vol. 10, no. 3, pp. 371–402, 2000.

[5] J. Schrimpf and L. E. Wetterwald, "Experiments towards automated sewing with a multi-robot system," in *Robotics and Automation (ICRA), 2012 IEEE International Conference on*. IEEE, 2012, pp. 5258–5263.

[6] T. Göpel, F. Härtl, A. Schneider, M. Buss, and H. Feussner, "Automation of a suturing device for minimally invasive surgery," *Surgical endoscopy*, vol. 25, no. 7, pp. 2100–2104, 2011.

[7] J. B. Adams, P. G. Schulam, R. G. Moore, A. W. Partin, and L. R. Kavoussi, "New laparoscopic suturing device: initial clinical experience," *Urology*, vol. 46, no. 2, pp. 242–245, 1995.

[8] J. C. Meade and G. I. Brecher, "Apparatus and method for minimally invasive suturing," Jul. 12 2011, uS Patent 7,976,555.

[9] D. T. Martin, "Circular needle applier with offset needle and carrier tracks," Jul. 26 2016, uS Patent 9,398,905.

[10] T.-J. Holwerda, "Surgical suture apparatus," Sep. 11 2014, uS Patent App. 14/238,704.

[11] B. Hu, S. S. Chung, L. C. Sun, K. Kawashima, T. Yamamoto, P. B. Cotton, C. J. Gostout, R. H. Hawes, A. N. Kalloo, S. V. Kantsevoy *et al.*, "Eagle claw ii: a novel endosuture device that uses a curved needle for major arterial bleeding: a bench study," *Gastrointestinal endoscopy*, vol. 62, no. 2, pp. 266–270, 2005.

[12] T. Looi, B. Yeung, M. Umasthan, and J. Drake, "Kidsarman image-guided pediatric anastomosis robot," in *Intelligent Robots and Systems (IROS), 2013 IEEE/RSJ International Conference on*. IEEE, 2013, pp. 4105–4110.

[13] S. Leonard, K. L. Wu, Y. Kim, A. Krieger, and P. C. Kim, "Smart tissue anastomosis robot (star): A vision-guided robotics system for laparoscopic suturing," *IEEE Transactions on Biomedical Engineering*, vol. 61, no. 4, pp. 1305–1317, 2014.

[14] A. Shademan, R. S. Decker, J. D. Opfermann, S. Leonard, A. Krieger, and P. C. Kim, "Supervised autonomous robotic soft tissue surgery," *Science translational medicine*, vol. 8, no. 337, pp. 337ra64–337ra64, 2016.

[15] B. Huang, A. Vandini, Y. Hu, S.-L. Lee, and G.-Z. Yang, "A vision-guided dual arm sewing system for stent graft manufacturing," in *Intelligent Robots and Systems (IROS), 2016 IEEE/RSJ International Conference on*. IEEE, 2016, pp. 751–758.

[16] B. Huang, M. Ye, Y. Hu, S.-L. Lee, A. Vandini, and G. Yang, "A multi-robot cooperation framework for sewing personalised stent grafts," *IEEE Transactions on Industrial Informatics*, 2017.

[17] B. Huang, M. Ye, S.-L. Lee, and G.-Z. Yang, "A vision-guided multi-robot cooperation framework for learning-by-demonstration and task reproduction," in *Intelligent Robots and Systems (IROS), 2017 IEEE/RSJ International Conference on*. IEEE, 2017, pp. 4797–4804.

[18] Y. Hu, L. Zhang, W. Li, and G.-Z. Yang, "Robotic sewing and knot tying for personalized stent graft manufacturing," in *Intelligent Robots and Systems (IROS), 2018 IEEE International Conference on*. IEEE, 2018.

[19] D. H. Myszka, *Machines and Mechanisms: Applied Kinematic Analysis*. Pearson Prentice Hall, 2005.

[20] S. Nemat-Nasser and W.-G. Guo, "Superelastic and cyclic response of niti sma at various strain rates and temperatures," *Mechanics of materials*, vol. 38, no. 5, pp. 463–474, 2006.

[21] C. Mattheck, "Teacher tree: The evolution of notch shape optimization from complex to simple," *Engineering Fracture Mechanics*, vol. 73, no. 12, pp. 1732–1742, 2006.

[22] G. Eggeler, E. Hornbogen, A. Yawny, A. Heckmann, and M. Wagner, "Structural and functional fatigue of niti shape memory alloys," *Materials Science and Engineering: A*, vol. 378, no. 1, pp. 24–33, 2004.

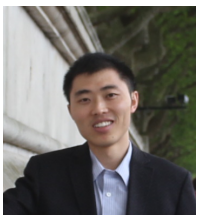

Yang Hu Yang Hu received his B.S. degree in Electronic Information Science and Technology from the College of Electronic Science and Engineering, Jilin University, Jilin, China. He received MRes in Medical Robotics and Image Guided Intervention and Ph.D. in Computer Science, both from the Hamlyn Centre, Imperial College London, U.K. His research interests include robotic suturing, snake-like surgical robot, compliant mechanism design and kinematic, dynamic modelling and control.

Lin Zhang Lin Zhang received his M.S degree in Computing Science in 2012, MRes degree in Medical Robotics and Image Guided Intervention in 2013, and PhD in Computer Science in 2018, all from Imperial College London, London, U.K. He is currently a research associate with Hamlyn Centre for Robotic Surgery, Imperial College London. His research interests include surgical vision, robotic surgery, visual servoing, image-guided intervention and machine learning.

Carlo Alberto Seneci Carlo Alberto Seneci graduated as an Industrial Automation Engineer (MEng, summa cum laude) from the University of Brescia in 2011. Following this, Carlo has been working for industry, whilst continuing with doctoral studies. In 2017 Carlo obtained a PhD in Robotic surgery at the Hamlyn Centre for Robotic Surgery (Imperial College London, UK).

Wei Li Wei Li is currently a Ph.D. candidate in medical robotics of the Hamlyn Centre for Robotic Surgery, Imperial College London, UK. He received his undergraduate degree in Aircraft Manufacturing from Harbin Institute of Technology, China in 2014, M.Sc. in Advanced Mechanical Engineering from University of Sheffield, U.K., and MRes. in Medical Robotics and Image Guided Intervention from Imperial College London, U.K.

Mohamed E. M. K. Abdelaziz Mohamed E. M. K. Abdelaziz received his B.Sc. (Highest Hons.) degree in mechatronics engineering from the German University in Cairo, Cairo, Egypt, in 2014 and the M.Sc. (cum laude) degree in robotics and mechatronics from the University of Twente, Enschede, The Netherlands, in 2016. He is currently working toward his Ph.D. in MR safe robotics at the Hamlyn Centre for Robotic Surgery, Imperial College London, London, U.K.

Professor Guang-Zhong Yang Professor Guang-Zhong Yang is director and co-founder of the Hamlyn Centre for Robotic Surgery, Imperial College London, UK. He is also the Chairman of the UK-RAS Network (http://ukras.org). Professor Yangs main research interests are in medical imaging, sensing and robotics. He is a Fellow of the Royal Academy of Engineering, fellow of IEEE, IET, AIMBE, IAMBE, MICCAI, CGI and a recipient of the Royal Society Research Merit Award.